

A Collective Excitation Interferometer for Rotation Sensing with a Trapped Bose-Einstein Condensate

G. Edward Marti,^{1,*} Ryan Olf,¹ and Dan M. Stamper-Kurn^{1,2}

¹*Department of Physics, University of California, Berkeley, California 94720, USA*

²*Materials Sciences Division, Lawrence Berkeley National Laboratory, Berkeley, California 94720, USA*

(Dated: May 31, 2022)

Compact inertial sensing schemes using trapped- and guided-atom interferometers have been unable to achieve high precision because of uncontrolled phase errors caused by trapping potentials and interactions. Here, we demonstrate an atom-shot-noise limited acoustic interferometer that uses sound waves in a toroidal Bose-Einstein condensate to measure rotations. Our system operates at $10^4 - 10^6$ times higher density and in a volume 10^9 times smaller than free-falling atom interferometers.

PACS numbers: 37.25.+k,03.75.-b,03.75.Kk,03.75.Dg

Keywords: matter wave interferometry, collective excitations, ring trap, toroidal trap, gyroscopy, Bose-Einstein condensates

Conventional atom interferometers measure acceleration [1] and rotation [2–4] by interfering dilute atomic wavepackets that traverse distinct paths in free fall [5]. The impressive sensitivity obtained by these devices scales with the area enclosed by the arms of the interferometer, leading to larger interferometers that average measurements on centimeter length scales [6]. Extending the capability of atom interferometers to probe shorter length scales could address fundamental questions, such as how gravity operates at short range; tackle practical problems, such as non-invasive material characterization; and aid in the development of miniaturized atomic sensors [7]. Trapped- or guided-atom interferometers may allow sensitive, localized inertial measurements by allowing interferometer arms to enclose the same area multiple times, gaining precision while remaining compact. However, for an atom interferometer to reach high signal-to-noise and probe short length scales, it is critical to develop an interferometric scheme compatible with high densities and realistic trapping potentials.

Trapped quantum degenerate gases offer a bright source for atom interferometry in small volumes, reaching densities of 10^{14} cm^{-3} that are at least four orders of magnitude higher than those utilized in free-falling-atom devices [6]. However, the price of high density is uncontrolled phase shifts and damped atomic motion, as seen in previous work that interfered single-atom states, such as momentum states in free fall [8, 9] or coherent states in a double-well potential [10, 11]. Also, in spite of high densities, the number flux of ultracold atoms through a trapped-atom interferometer is typically far lower than that achieved in unguided-atom setups, making it highly desirable that the readout noise of such interferometers reach, or even surpass [12–15], the atom-shot-noise limit.

Here, we demonstrate a proof-of-principle rotation sensor by interfering collective excitations of a dense, trapped sample. This approach produces a signal nominally insensitive to density and whose systematic biases

are suppressed by atom-atom interactions. Specifically, we measure rotation using acoustic standing waves in a toroid-shaped atomic superfluid, in a manner similar to that used in the hemispherical resonator gyroscope [16]. The rotation sensitivity achieved in this work is modest, but our results demonstrate several key advantages of collective-excitation interferometry. As collective modes of an interacting Bose-Einstein condensate (BEC), sound waves can propagate over long distances. Interactions in a superfluid can enhance the lifetime of the sound mode even in the presence of disorder [17] and suppress systematic biases that arise from weak disorder in the potential. In addition, time reversal symmetry guarantees that linear forces, atom number variations, interaction energy shifts, and trap inhomogeneities cannot distinguish counter-propagating acoustic modes; these effects primarily introduce common-mode phase shifts that do not deteriorate the signal. Further, the irrotational nature of the superfluid provides a non-rotating frame for the propagating sound waves, against which the slow rotation of an observer can be measured absolutely. Finally, our sensor is compact, with a linear dimension of $60 \mu\text{m}$ and volume of $5 \times 10^{-9} \text{ cm}^3$. Extending this work to circular waveguides of millimeter dimensions [18] could improve sensitivity at the expense of compactness.

Low-order collective modes have been used in the past to measure Casimir-Polder forces [19] and to measure the circulation induced by a vortex in a BEC [20–22]. We extend this work by using higher-order standing-wave acoustic modes to increase sensitivity, overcome technical noise limitations, and reach atom-shot-noise-limited detection of rotations at atomic densities 10^4 times higher, and within a volume 10^9 times smaller, than in free-space atom interferometers [23, 24].

In our experiment, we prepare a degenerate, spin-polarized gas of ^{87}Rb in a far-detuned optical dipole trap, following a procedure similar to that of Ref. 25. We then transfer the atoms into an overlain toroidal optical po-

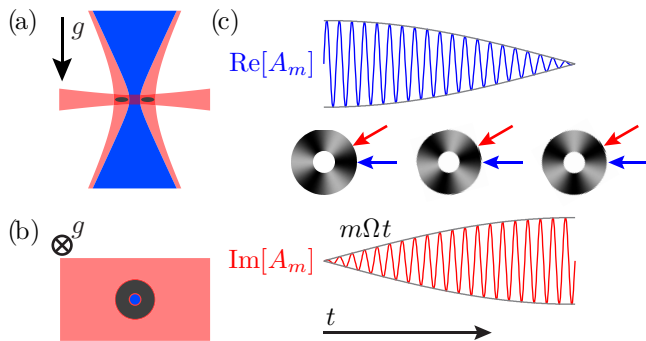


FIG. 1. Three laser ring trap viewed from the side (a) and top (b). A standing acoustic wave oscillates at its eigenfrequency (c) with fast density oscillation at the antinode ($\text{Re}[A_m]$, blue arrow and curve) and no amplitude at the node ($\text{Im}[A_m]$, red arrow and curve). As the orientation of the mode rotates, the envelope (gray) of the imaginary component linearly increases in proportion to the rotation rate and mode number. Density shifts should not alter this envelope, which constitutes the rotation signal.

tential formed by the intersection of three light beams (Fig. 1(a), (b)). An attractive light sheet, with an optical power of 3 mW, a wavelength of $\lambda = 836$ nm, and an elliptical focus with $1/e^2$ radii of $10.5 \mu\text{m}$ and $400 \mu\text{m}$, confines atoms to a horizontal plane. An annular potential, created by coaxial attractive ($400 \mu\text{W}$, $\lambda=830$ nm, $1/e^2$ radius of $26 \mu\text{m}$) and repulsive (3 mW, $\lambda=532$ nm, $1/e^2$ radius of $11 \mu\text{m}$) light beams that propagate vertically, provides in-plane confinement. To maximize the stability of the optical system, we deliver the coaxial vertical beams via the same large-mode-area fiber. We adjust the alignment and beam radii at the trap location using a telescope with adjustable axial and lateral chromatic shifts. The optical potential minimum lies in a circle of radius $16 \mu\text{m}$, about which the atoms experience radial and vertical trap frequencies of $(\omega_z, \omega_r) = 2\pi \times (260, 86)$ Hz. Evaporative cooling from the optical potential yields samples with 4×10^4 condensed atoms and no discernible thermal fraction, Thomas-Fermi radii of $6 \mu\text{m}$ and $1.5 \mu\text{m}$ in the radial and vertical directions, respectively, and a chemical potential of $\mu = h \times 700$ Hz. Similar optical ring traps have been demonstrated previously, albeit with different optical setups [26–28].

The excitations of a cylindrically symmetric medium may be characterized by the integer azimuthal quantum number m , as well as the transverse (radial and axial) quantum numbers. We excite a specific superposition of the $\pm m$ lowest-transverse-order sound modes by applying an additional optical potential to the trapped BEC that establishes an initial density modulation with high spatial overlap with the selected mode. To create this potential, we illuminate a chrome optical mask of an m -fold propeller pattern (Fig. 2(e), icons) with a $400 \mu\text{W}$, $\lambda=532$ nm laser. The masked light is then imaged onto

the plane of the trapped atoms, using a 1:10 imaging system with a resolution of $3 \mu\text{m}$, creating a repulsive optical potential. After evaporative cooling to the final atom number and temperature, the light is suddenly extinguished and the perturbed condensate evolves freely for a variable hold time t , at which point it is destructively imaged.

We measure the *in situ* condensate density with a high signal-to-noise absorption imaging protocol. We first reduce the optical density of the gas by exciting only 10%–25% of the atoms to the $|F=2\rangle$ ground hyperfine state with a short ($20 \mu\text{s}$), weak (2% of saturation intensity) light pulse detuned by about 5 linewidths from the $|F=1\rangle \rightarrow |F=2\rangle$ D2 transition. Detuning the light from resonance ensures that the sample is uniformly excited because it is optically thin. We then apply a resonant probe pulse to the cycling transition for $50 \mu\text{s}$ at saturation intensity [29] and image the unscattered light onto a CCD camera. We found this approach to give greater sensitivity than dispersive imaging.

The acoustic excitations reveal themselves as oscillating standing waves of the condensate density. From the measured column density distribution $\tilde{n}(x, y)$, we extract the azimuthal spatial Fourier coefficient

$$A_m = \frac{\int_{r < r_c} dx dy \tilde{n} e^{im\phi}}{\int_{r < r_c} dx dy \tilde{n}}, \quad (1)$$

up to a cutoff radius $r_c = 40 \mu\text{m}$, where the atomic density is zero [30]. A_m is a complex number whose phase indicates the angular position of the standing wave and whose amplitude indicates the strength of the density modulation. Fig. 3(a) shows the evolution of $A_3(t)$ for condensates prepared with the $m=3$ mask at various initial orientations, with one datum obtained per experimental cycle.

The excitation and read-out schemes are highly selective. The m -fold propeller produces strong excitation of the m -node standing wave, along with a weak residual excitation of the $(m \pm 1)$ -node standing waves due to slight misalignment of the center of the mask to the center of the trap (Fig 3(b)). The spatial mode pattern $\delta\tilde{n}(x, y)$ of the standing-wave excitation can be measured by fitting the pixel-by-pixel temporal record $\tilde{n}(x, y, t)$ to $\tilde{n}_0(x, y) + \delta\tilde{n}(x, y) e^{\Gamma t} \cos \omega(t - t_0)$, where Γ , ω , and t_0 are fixed from a fit to A_m (Fig. 2(a-d)).

The observed standing-wave mode frequencies agree well with their predicted values and demonstrate the expected linear phonon dispersion relation. The acoustic eigenfrequencies of a tubular medium of circumference L , an approximation for the toroid, are $f = mc_{\text{eff}}/L$, where c_{eff} is the effective speed of sound in the channel. The linear scaling is seen for the $m=2$ through $m=6$ modes, with $c_{\text{eff}} = 1.29(2)$ mm/s for $L = 2\pi \times 16 \mu\text{m}$ in Fig. 2(e). The $m=7$ mode is perturbed by the first excited radial mode, as expected when the acoustic wave-

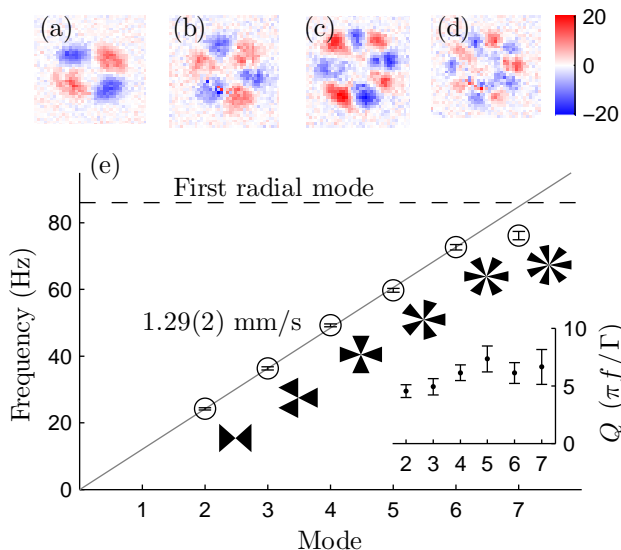


FIG. 2. Spatial profiles of the $m=2$ (a) through 5 (d) eigenmodes are calculated from each pixel’s temporal record. Each profile shows a field of view of $90 \times 90 \mu\text{m}^2$. Color scale is the amplitude in number of atoms. (e) Eigenfrequencies show the expected linear trend for modes $m=2-6$, shown as the diagonal gray line. A large negative shift of mode $m=7$ is expected from coupling to the first radial mode. The inset shows the Q factor for each mode.

length approaches the radial extent of the gas. In particular, the mode frequency is reduced as the mode-pattern becomes concentrated at the outer edge of the ring, increasing L and lowering c_{eff} .

Surprisingly, the measured lifetimes of the sound waves are short compared to previous experiments (inset of Fig. 2(e)), most likely due to collisions with a small, non-condensed fraction [31, 32]. We note that a toroidal potential has a larger noncondensed fraction than a three-dimensional harmonic trap at the same reduced temperature (T/T_c , where T_c is the transition temperature).

To sense rotations, we look for precession in the orientation of the standing acoustic mode. In a smooth ring, the standing wave orientation remains fixed in the inertial frame and precesses in the rotating lab frame, like a Foucault pendulum [33], as the clockwise ($-m$) and counterclockwise ($+m$) propagating modes appear to be split in frequency by the rotation.

In contrast, static trap distortions couple the $\pm m$ modes, introducing a frequency splitting between the sine- and cosine-like m -node density modulations measured by A_m . For instance, in a ring of radius r , a static potential perturbation with azimuthal dependence $V(\theta) = \text{Re}[\sum_m V_m e^{im\theta}]$ yields (to first order in V_m) a frequency splitting between the two m -node standing acoustic modes of $|\delta_m| \propto (|V_{2m}|/\hbar)(\xi/\lambda)$, where $\xi \propto n^{-1/2}$ is the healing length [34], n is the atomic density, and

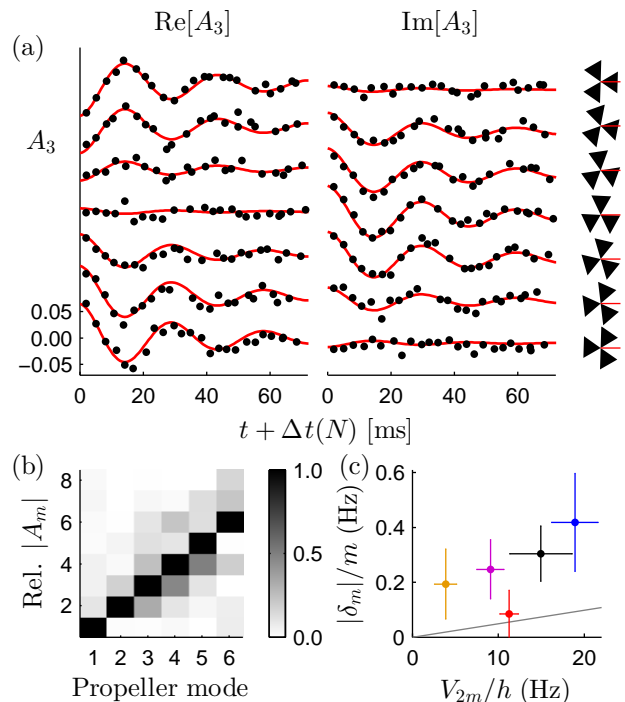


FIG. 3. (a) Real (left) and imaginary (right) components of A_3 oscillate in time. In each row, relative amplitudes correspond, with $2\pi/3$ periodicity, to the angular orientation of the excitation mask (schematic, far right). Data are offset for clarity. (b) Relative response of A_m as a function of mode number for each propeller. The applied mode always has the strongest response, but neighboring modes are weakly excited by a slight misalignment of the mask. Each column is scaled to its peak response. (c) Frequency splitting $|\delta_m|$ of mode m versus the trap distortion $V_{2m}/h = 2A_{2m,0}\mu/h$. The gray line is the expected mean-field result $\delta_m/m = V_{2m}\xi/3.8r$ for distortions in our anharmonic waveguide.

λ is the acoustic wavelength. The effects of such distortions are thus suppressed by the high density of the atomic medium; for our system, the suppression factor is $\xi/\lambda \simeq 50$ (Fig. 3(c)).

Moreover, the influences of rotation and of trap distortions on the $\pm m$ acoustic modes are distinct, akin to the separate effects of circular and linear birefringence, respectively, on the polarization of light. To quantify each influence, we excite each mode $m=2$ through 6 at a large number of angles (a small selection is shown in Fig. 3(a)), and fit the data at each m to a three-mode (unperturbed superfluid and its $\pm m$ acoustic excitations) model of the temporal evolution. From this fit, we obtain the frequency difference and principal axes (i.e. the magnitude and phase of δ_m) selected by the static trap distortion (Fig. 4, top). The measured frequency differences are limited by statistical fluctuations and consistent with the small distortion of the trapped gas measured from static images.

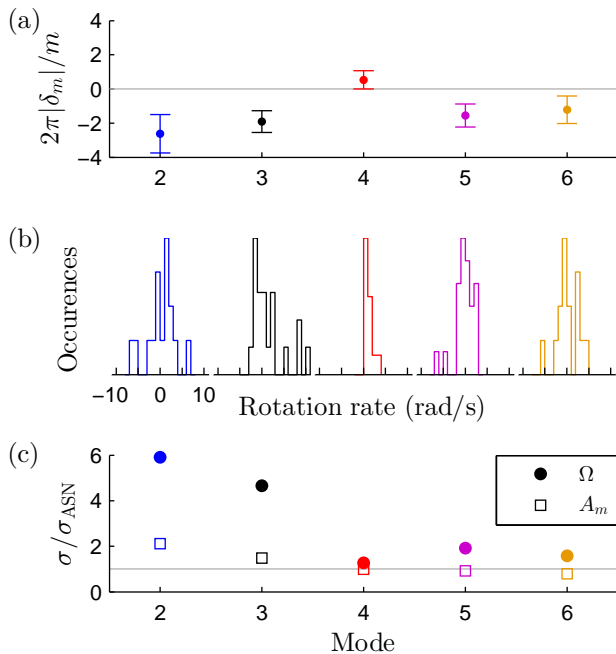


FIG. 4. (a) The frequency splitting is determined by fitting, on average, 500 images and 18 orientations of the optical mask per mode to a three-mode dynamical model. Error bars are determined from a jackknifing procedure that excludes a single orientation from the dataset. The units here, in radians per second per mode number, can be compared directly to the measured rotation rate. (b) Rotation estimates are binned in 1 rad/s intervals. Each value is the result of a fit to the rotation rate for ~ 30 points taken at each orientation of the optical mask. (c) The standard error σ of the rotation estimates (closed circles) and noise in each component of A_m (open squares) are close to the atom-shot-noise limit σ_{ASN} for modes $m=4-6$. Modes $m=2$ and 3 show an excess of noise, most likely from technical fluctuations in the toroidal potential.

To extract a rotation rate, we fit the data at each mask orientation (~ 30 points, corresponding to a row in Fig. 3(a)) to a prediction of the sound wave evolution in a rotating frame, plotted as a histogram in Fig. 4(b). The only free parameters are the rotation rate and the amplitude of the initial excitation. Mechanical properties of the system such as the frequency, frequency splitting, and phase are fixed from fits to the rest of the data set.

The measured rotation noise of several rad/s matches well with the expected atom-shot-noise limit (Fig. 4, bottom). In imaging the distribution of N uncorrelated atoms, atom-shot-noise yields an uncertainty $\Delta A_m = (2N)^{-1/2}$ in extracting either the real or imaginary component of A_m in a single run. The measured rotation rate then acquires an uncertainty of $\Delta\Omega_{ASN} = a\Gamma/(mp\sqrt{NN_r})$, where Γ is the decay rate of the standing wave, p is the fractional density modulation excited in operating the interferometer, and N_r is the number of

independent experimental realizations. The prefactor a depends on how measurements are distributed in time; here, $a = 3.2$ for evolution times sampled uniformly between 0 and $2/\Gamma$. For measurements using the higher-order sound modes, the reduced technical noise in our images at higher spatial frequencies allows us to achieve the atomic shot-noise limit (Fig. 4(c)). Unfortunately, because the quality factor of acoustic standing-wave oscillations is found to be roughly independent of the mode number, the use of higher order modes does not improve sensitivity in our apparatus beyond overcoming technical noise.

The measurement noise of a free-space atom interferometer can be written in a form similar to $\Delta\Omega_{ASN}$ above: $\Delta\Omega_{free} = T^{-1}/(4\pi(L/\lambda)\sqrt{N})$, where L is the distance between interaction regions, λ is the wavelength of the optical or material grating used as an atomic beam splitter, and T is the atomic travel time between beam splitters. Written this way, our acoustic interferometer acts as a device that measures how far a feature of azimuthal size $\lambda/L \sim 1/m$ rotates over a time $1/T \sim \Gamma$.

For a trapped atom sample to reach sensitivities competitive to free-space interferometers, short wavelengths (higher m), large atom numbers, and long propagation times are required. In our current setup, both atom number and m are limited by the small size of our ring. However, rings have been demonstrated with $\approx 10^4$ greater enclosed area [18]. In future work we hope to understand and minimize the damping of the acoustic modes.

Collective excitation interferometry circumvents many common problems associated with trapped-atom interferometry, and allows for the operation of robust, low-bias inertial sensors with densities $10^4 - 10^6$ times greater than traditional free-falling interferometers in a volume 10^9 times smaller. Even at current levels of sensitivity, collective mode gyroscopy can serve as a direct probe of the rotation of the ground state [35]. For example, we are sensitive to rotation rates corresponding to a single trapped vortex with $\Omega_v = \hbar/mr^2 = 3 \text{ rad s}^{-1}$, which is the rotation scale of simple spin-orbit effects in dressed-atom systems [36].

We thank A. Öttl and M. Solarz for help with designing and building the cold atom setup and G. Dunn and S. Lourette for technical assistance. This work was supported by the Defense Advanced Research Project Agency (Grant No. 49467-PHDRP) and the Defense Threat Reduction Agency (Contract No. HDTRA1-09-1-0020). GEM acknowledges support from the Hertz Foundation.

* emarti@berkeley.edu

[1] J. M. McGuirk, G. T. Foster, J. B. Fixler, M. J. Snadden, and M. A. Kasevich, Phys. Rev. A **65**, 033608 (2002).

- [2] T. L. Gustavson, P. Bouyer, and M. A. Kasevich, *Phys. Rev. Lett.* **78**, 2046 (1997).
- [3] T. L. Gustavson, A. Landragin, and M. A. Kasevich, *Classical and Quantum Gravity* **17**, 2385 (2000).
- [4] D. S. Durfee, Y. K. Shaham, and M. A. Kasevich, *Phys. Rev. Lett.* **97**, 240801 (2006).
- [5] A. D. Cronin, J. Schmiedmayer, and D. E. Pritchard, *Rev. Mod. Phys.* **81**, 1051 (2009).
- [6] H. Müller, S. W. Chiow, Q. Long, S. Herrmann, and S. Chu, *Phys. Rev. Lett.* **100**, 180405 (2008).
- [7] Daniel M. Farkas, Kai M. Hudek, Evan A. Salim, Stephen R. Segal, Matthew B. Squires, and Dana Z. Anderson, *Appl. Phys. Lett.* **96**, 093102 (2010).
- [8] Y.-J. Wang, D. Z. Anderson, V. M. Bright, E. A. Cornell, Q. Diot, T. Kishimoto, M. Prentiss, R. A. Saravanan, S. R. Segal, and S. Wu, *Phys. Rev. Lett.* **94**, 090405 (2005).
- [9] O. Garcia, B. Deissler, K. J. Hughes, J. M. Reeves, and C. A. Sackett, *Phys. Rev. A* **74**, 031601 (2006).
- [10] Y. Shin, M. Saba, T. A. Pasquini, W. Ketterle, D. E. Pritchard, and A. E. Leanhardt, *Phys. Rev. Lett.* **92**, 050405 (2004).
- [11] G.-B. Jo, Y. Shin, S. Will, T. A. Pasquini, M. Saba, W. Ketterle, D. E. Pritchard, M. Vengalattore, and M. Prentiss, *Phys. Rev. Lett.* **98**, 030407 (2007).
- [12] J. Esteve, C. Gross, A. Weller, S. Giovanazzi, and M. K. Oberthaler, *Nature (London)* **455**, 1216 (2008).
- [13] J. Appel, P. J. Windpassinger, D. Oblak, U. B. Hoff, N. Kjrgaard, and E. S. Polzik, *Proc. Natl. Acad. Sci.* **106**, 10960 (2009).
- [14] I. D. Leroux, M. H. Schleier-Smith, and V. Vuletić, *Phys. Rev. Lett.* **104**, 073602 (2010).
- [15] M. H. Schleier-Smith, I. D. Leroux, and V. Vuletić, *Phys. Rev. Lett.* **104**, 073604 (2010).
- [16] D. M. Rozelle, in *Spaceflight Mechanics*, Advances in the Astronautical Sciences, Vol. 134, edited by A. M. Segerman, P. C. Lai, M. P. Wilkins, and M. E. Pittelkau, American Astronautical Society (Univelt, Inc., 2009) Proceedings of the 19th AAS/AIAA Space Flight Mechanics Meeting.
- [17] D. Dries, S. E. Pollack, J. M. Hitchcock, and R. G. Hulet, *Phys. Rev. A* **82**, 033603 (2010).
- [18] S. Gupta, K. W. Murch, K. L. Moore, T. P. Purdy, and D. M. Stamper-Kurn, *Phys. Rev. Lett.* **95**, 143201 (2005).
- [19] D. M. Harber, J. M. Obrecht, J. M. McGuirk, and E. A. Cornell, *Phys. Rev. A* **72**, 033610 (2005).
- [20] A. E. Leanhardt, A. Görlitz, A. P. Chikkatur, D. Kielpinski, Y. Shin, D. E. Pritchard, and W. Ketterle, *Phys. Rev. Lett.* **89**, 190403 (2002).
- [21] M. Cozzini, S. Stringari, V. Bretin, P. Rosenbusch, and J. Dalibard, *Phys. Rev. A* **67**, 021602 (2003).
- [22] V. Bretin, P. Rosenbusch, F. Chevy, G. V. Shlyapnikov, and J. Dalibard, *Phys. Rev. Lett.* **90**, 100403 (2003).
- [23] P. Treutlein, K. Y. Chung, and S. Chu, *Phys. Rev. A* **63**, 051401 (2001).
- [24] H. Müller, S. W. Chiow, S. Herrmann, S. Chu, and K.-Y. Chung, *Phys. Rev. Lett.* **100**, 031101 (2008).
- [25] Y.-J. Lin, A. R. Perry, R. L. Compton, I. B. Spielman, and J. V. Porto, *Phys. Rev. A* **79**, 063631 (2009).
- [26] K. Henderson, C. Ryu, C. MacCormick, and M. G. Boshier, *New J. of Phys.* **11**, 043030 (2009).
- [27] A. Ramanathan, K. C. Wright, S. R. Muniz, M. Zelan, W. T. Hill, C. J. Lobb, K. Helmerston, W. D. Phillips, and G. K. Campbell, *Phys. Rev. Lett.* **106**, 130401 (2011).
- [28] S. Moulder, S. Beattie, R. P. Smith, N. Tammuz, and Z. Hadzibabic, *Phys. Rev. A* **86**, 013629 (2012).
- [29] G. Reinaudi, T. Lahaye, Z. Wang, and D. Guéry Odelin, *Opt. Lett.* **32**, 3143 (2007).
- [30] The center of the polar coordinates is determined by fitting each image to an ideal toroidal Thomas-Fermi with a dipole angular perturbation.
- [31] D. S. Jin, M. R. Matthews, J. R. Ensher, C. E. Wieman, and E. A. Cornell, *Phys. Rev. Lett.* **78**, 764 (1997).
- [32] D. M. Stamper-Kurn, H.-J. Miesner, S. Inouye, M. R. Andrews, and W. Ketterle, *Phys. Rev. Lett.* **81**, 500 (1998).
- [33] L. Foucault, *Comptes rendus hebdomadaires des seances de l'Academie des Sciences* **32**, 135 (1851).
- [34] F. Dalfovo, S. Giorgini, L. P. Pitaevskii, and S. Stringari, *Rev. Mod. Phys.* **71**, 463 (1999).
- [35] F. Chevy, K. W. Madison, and J. Dalibard, *Phys. Rev. Lett.* **85**, 2223 (2000).
- [36] N. R. Cooper, *Phys. Rev. Lett.* **106**, 175301 (2011).